Tidal signatures in sporadic E occurrence rates: migrating and nonmigrating components

Jacobi, Ch.[1], Lilienthal, F.[1], Yamazaki, Y.[2], Sobhkhiz-Miandehi, S.[2], Arras, C.[3]

[1] *Institute for Meteorology, Leipzig University, Stephanstr. 3, 04103 Leipzig, Germany, E-mail: jacobi@uni-leipzig.de*
[2] *Helmholtz Centre Potsdam German Research Centre for Geosciences - GFZ, Section 2.3: Geomagnetism, Telegrafenberg, 14473 Potsdam, Germany*
[3] *Helmholtz Centre Potsdam German Research Centre for Geosciences - GFZ, Section 1.1: Space Geodetic Techniques, Telegrafenberg, 14473 Potsdam, Germany*

Summary: We analyze sporadic E (E_S) occurrence rates (OR) obtained from ionospheric GPS radio occultation measurements by the FORMOSAT-3/COSMIC constellation. Maximum OR are seen at 95 – 105 km altitude. Midlatitude E_S are mainly due to wind shear in the presence of tides, and the strongest signals are the migrating diurnal and semidiurnal components. Especially in the Southern Hemisphere, nonmigrating components such as a diurnal westward wave 2 and a semidiurnal westward wave 1 are also visible, especially at high latitudes. Near the equator, a strong diurnal eastward wavenumber 3 component and a semidiurnal eastward wavenumber 2 component occur in summer and autumn. Terdiurnal and quarterdiurnal components are weaker than the diurnal and semidiurnal ones.

Zusammenfassung: Wir untersuchen Auftrittsraten sporadischer E-Schichten (E_S), die aus ionosphärischen GPS-Radiookkultationsmessungen von FORMOSAT-3 / COSMIC bestimmt wurden. Maximale Auftrittsraten treten in 95 – 105 km Höhe auf. E_S in mittleren Breiten sind hauptsächlich auf Windscherung durch Gezeiten zurückzuführen, und die stärksten Signale sind eine westwärts wandernde Tages- und Halbtageskomponente. Insbesondere in der Südhemisphäre sind auch nichtmigrierende Komponenten wie eine ganztägige westwärts wandernde Welle der Wellenzahl 2 und eine halbtägige westwärts wandernde Welle der Wellenzahl 1 sichtbar. In der Nähe des Äquators treten im Sommer und Herbst eine starke ostwärts wandernde ganztägige Komponente der Wellenzahl 3 und eine ostwärts wandernde halbtägige Komponente der Wellenzahl 2 auf. Dritteltägige und vierteltägige Komponenten sind schwächer als die ganz- und halbtägigen.

1 Introduction

Sporadic E (E_S) layers are thin clouds of accumulated ions in the lower ionosphere. They are most frequently found during the summer season at middle latitudes (e.g., Arras et al., 2008). E_S are generally formed at heights between 90 km and 120 km. Their occurrence can be described through the wind shear theory (Whitehead, 1961), which describes the

interaction between the metallic ion concentration, the Earth's magnetic field, and the vertical shear of the neutral wind (e.g., Gong et al., 2014; Fytterer et al., 2014).

The dynamics of the lower thermosphere at time scales up to one day are mainly influenced by solar tides, with periods of a solar day and its harmonics (e.g., Forbes, 1995). Tidal amplitudes usually maximize around or above 120 km, where they are of the order of magnitude of the mean wind. Shorter period tidal waves often have smaller amplitudes, so that, on a global scale, the major diurnal variability of lower thermosphere winds is due to the diurnal tide (DT, Pancheva et al., 2002), the semidiurnal tide (SDT, Jacobi et al., 1999; Pancheva et al., 2002), and, to a lesser degree, also to the terdiurnal tide (TDT, Beldon et al., 2006; Liu et al., 2019). Note, however, that at higher midlatitudes the DT wind amplitudes become small compared with SDT ones during most of the year. Owing to its smaller amplitude, the quarterdiurnal tide (QDT) has been analyzed less frequently in the past, but more recently has attained increasing attention (Liu et al., 2015; Azeem et al., 2016; Jacobi et al., 2018a, 2019; Guharay et al., 2018).

Solar tides are a major source of vertical wind shear, and the tidal contribution to the overall wind shear is frequently larger than the one of the background wind. Therefore, tide-like structures are also expected in E_S occurrence rates. Consequently, tides are generally accepted to be the major driver of E_S (Mathews, 1998), and they lead to the downward moving tidal signatures in ionosonde registrations (e.g., Haldoupis et al., 2006; Haldoupis, 2012). Analyzing GPS E_S observations together with meteor radar wind measurements at Collm (51.3°N, 13.0°E), a clear correspondence of E_S and negative wind shear maximums has been found for the SDT (Arras et al., 2009), TDT (Fytterer et al., 2013), and QDT (Jacobi et al., 2019), but not for the DT (Jacobi and Arras, 2019). Fytterer et al. (2014) and Jacobi et al. (2019) compared GPS E_S radio occultations (RO) and modeled wind shear. They demonstrated the similarity of the TDT and QDT in E_S and wind shear on a global scale. Resende et al. (2018a) modeled the connection of E_S and tides, although focusing on the equatorial region, where electric field effects become more important than at middle latitudes.

Comparisons of E_S and wind shear have frequently been performed based on local wind measurements (Arras et al., 2009; Fytterer et al., 2013; Jacobi et al., 2019; Jacobi and Arras, 2019). These observations cannot distinguish between migrating and non-migrating tidal components. To reveal the migrating E_S tidal components only, these results were compared with E_S sampled in local time at all longitudes. This approach showed good correspondence for Northern Hemisphere (NH) stations, where the migrating tidal component is obviously dominating.

Using frequency-wavenumber analysis, it is possible to analyze also non-migrating tidal components from global fields. Therefore, in the following, we present analyses of migrating but also non-migrating tides seen in E_S OR, which are based on FORMOSAT-3/COSMIC GPS RO observations. We will use the following notation: The period is represented by the letter D, S, T, Q for diurnal, semidiurnal, terdiurnal, and quarterdiurnal, respectively. This is followed by W or E for westward or eastward, and an integer representing the zonal wavenumber. So DW1 represents the diurnal westward migrating tide of zonal wavenumber 1, SE2 stands for the semidiurnal eastward wavenumber 2 component, and so forth.

Note that the correspondence between the wind shear and the E_S diurnal variability is much weaker for the DT than for the SDT, TDT, and QDT. This is owing to the fact

that a diurnal E_S variation is not only due to wind shear, but also owing to background ionization, which is much stronger during daytime. Strictly speaking, it is therefore incorrect to interpret the diurnal E_S variation as a DT signature. For a consistent description, we nevertheless refer to the diurnal E_S signature as a DT.

2 Sporadic E analysis

We make use of ionospheric RO measurements by the FORMOSAT-3/COSMIC constellation, which performs observations in both the neutral and ionized atmosphere (Anthes et al., 2008) though a constellation of six low-Earth orbiting (LEO) satellites. During each occultation, signals of the rising or setting GPS satellites are received by a LEO satellite. When the signals pass the atmosphere/ionosphere of the Earth, they are influenced in particular by the ionospheric electron density, which causes refraction and degradation of the GPS waves. This effect can be utilized to obtain information about the ionosphere. Observation of the neutral atmosphere is also possible, but this is not the topic of this study. Detailed information on the RO technique principles is provided by Hajj et al. (2002) and Kursinski et al. (1997).

In this study the Signal-to-Noise (SNR) profiles of the GPS L1 phase measurements are used according to Arras and Wickert (2018). The SNR is very sensitive to vertical variations of the electron density, and these occur within an E_S layer. These vertically localized electron density variations lead to phase fluctuations of the GPS signal, which can be observed as changes in the received signal strength (Hajj et al., 2002). In order to avoid influences from the different basic signal power values on the further data analysis, every SNR profile is normalized first. In the case of the absence of ionospheric disturbances, the SNR value is almost constant at altitudes above 35 km. The SNR standard deviation profile is considered to be disturbed when it exceeds an empirically found threshold of 0.2. If large standard deviation values are concentrated within a thin layer of less than 10 km vertical extent, we assume that the respective SNR profile includes the signature of an E_S layer. The height where the SNR value deviates most from the mean of the SNR profile is considered as the altitude of the E_S layer. This has been validated by comparisons with ionosonde E_S observations. (Arras and Wickert, 2018; Resende et al., 2018b).

The following analysis is based on observations from 2007 to 2017. The number of occultations and the number of observed E_S are each binned into a 4-dimensional grid of $5° \times 10° \times 1\text{km} \times 1\text{h}$ (latitude $\times$ longitude $\times$ altitude $\times$ time), calculated within partly overlapping boxes of 10° (latitudes, 20° (longitude), 10 km (altitude) and 1 h, respectively, and as 3-monthly (seasonal) means. E_S OR are then calculated as the number of E_S divided by the number of occultations in each bin. Note that the OR of an individual bin is set to zero if there are less than five occultations within this bin.

3 Global distribution of Sporadic E

Figure 1 shows the 2007 - 2017 mean zonal mean and seasonal mean E_S OR for December–February (DJF), and June–August (JJA). The distributions are similar to those shown by Fytterer et al. (2014); Jacobi et al. (2019) obtained from a more limited dataset.

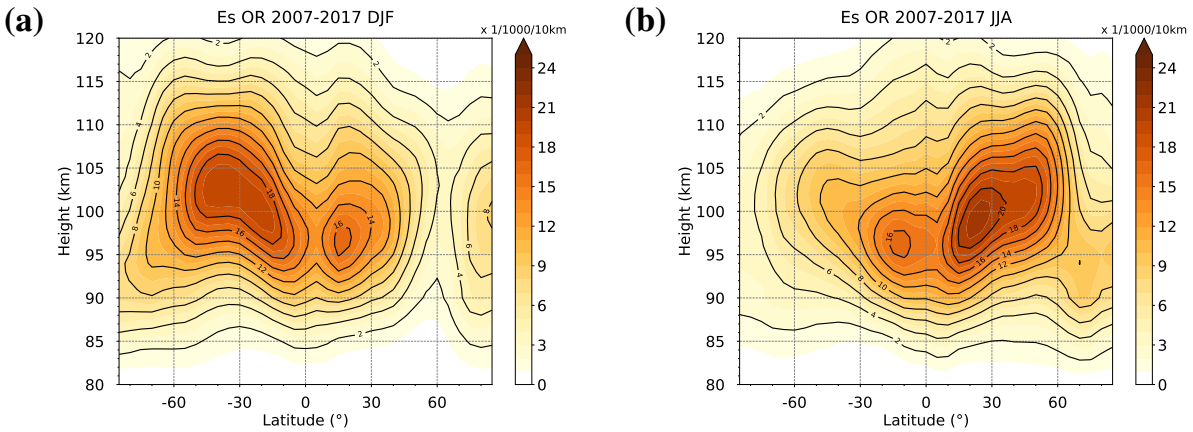

Figure 1: *Zonal and seasonal mean E_S occurrence rates in a 10 km vertical window each for (a) DJF, (b) JJA. Data are averages over* 2007 - 2017.

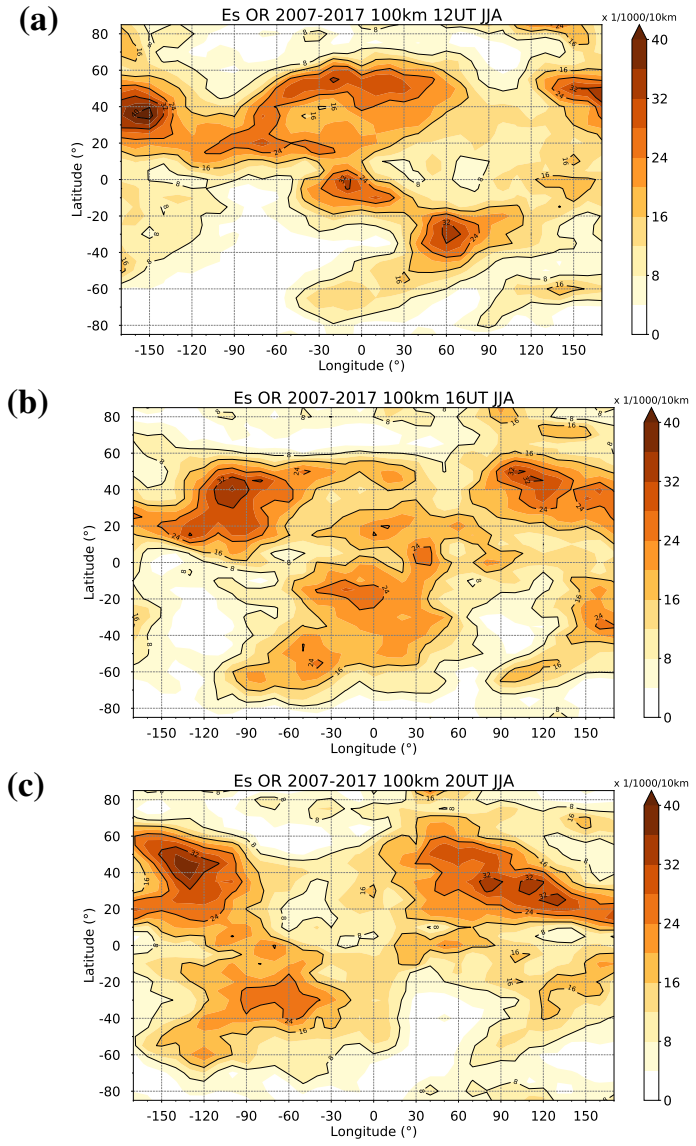

Figure 2: *Global distribution of JJA mean E_S occurrence rates at 95 – 105 km for (a) 12 UT, (b) 16 UT, (c) 20 UT.*

Maximum OR are found at altitudes slightly between 95 km and 105 km. OR maximize in summer, which is thought to be owing to increased meteor influx during that season (Haldoupis et al., 2007). The summer maximum is more pronounced in the NH, which is due to the weaker magnetic field within the South Atlantic Anomaly (e.g., Arras et al., 2008; Chu et al., 2014; Arras and Wickert, 2018). Near the equator, E_S OR are small, owing to the horizontal magnetic field at the magnetic equator, which does not allow the electrons to follow the vertically moving ions (e.g., Arras et al., 2008, 2010; Arras and Wickert, 2018).

As an example of the diurnal variability of JJA mean E_S, Figure 2 presents latitude-longitude sections of OR in an 10 km height window centered at 100 km, for three different universal times differing by 4 hrs each. The data have been sampled in windows of 10° latitude and 20° longitude. The strong summer signal is visible between 10 and 20°N, and it exhibits a clear wavenumber 2 signature at midlatitudes. This structure is moving westward with time, and obvious is the signature of the migrating SW2. The SW2 is also visible in the Southern Hemisphere (SH). At the equator, the semidiurnal signal is only weakly visible.

4 Spectral distribution of tidal components

In order to analyze the tidal components in the long-term diurnal E_S signal, we performed frequency-wavenumber (f-k) analyses that have been based on gridded data that have again been sampled in boxes of 10° times 20° in latitude and longitude, resp., and 10 km in height. Again, we analyze results in windows centered at 100 km. Figure 3 presents f-k spectra at 30°N, while the spectra for 30°S are shown in Figure 4.

In the NH, the main signal is due to the DW1 and SW2. In winter, OR are small

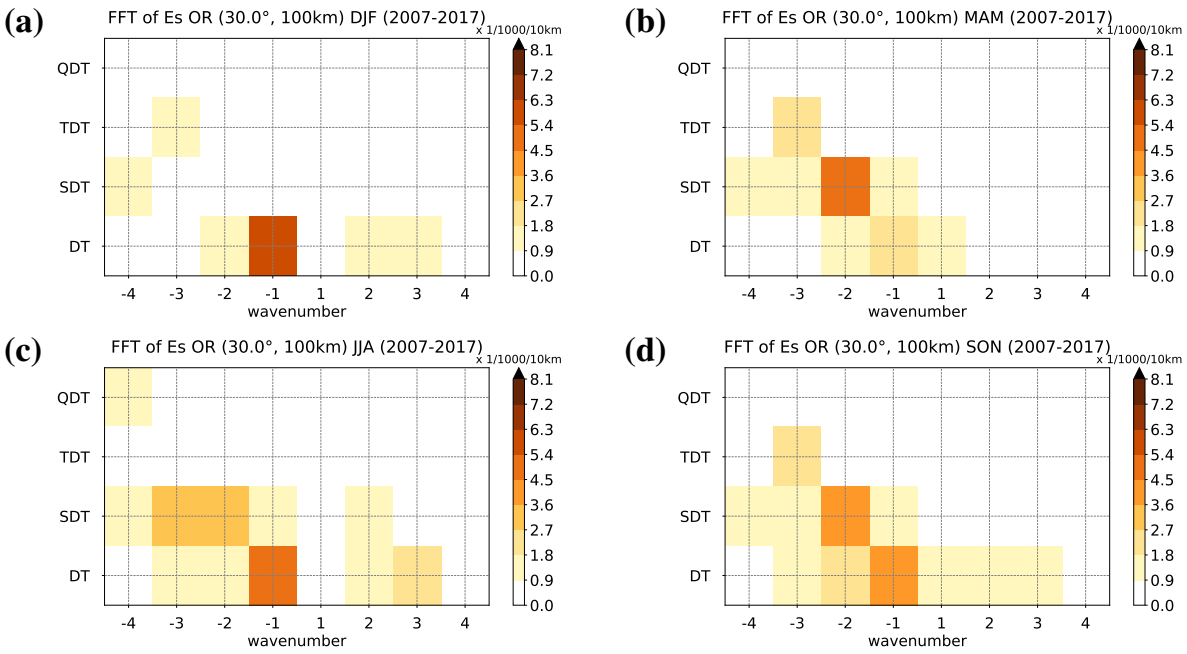

Figure 3: *Wavenumber-frequency spectra of E_S OR at 30°N in the 95 – 105 km height window for (a) DJF, (b) MAM, (c) JJA, and (d) SON.*

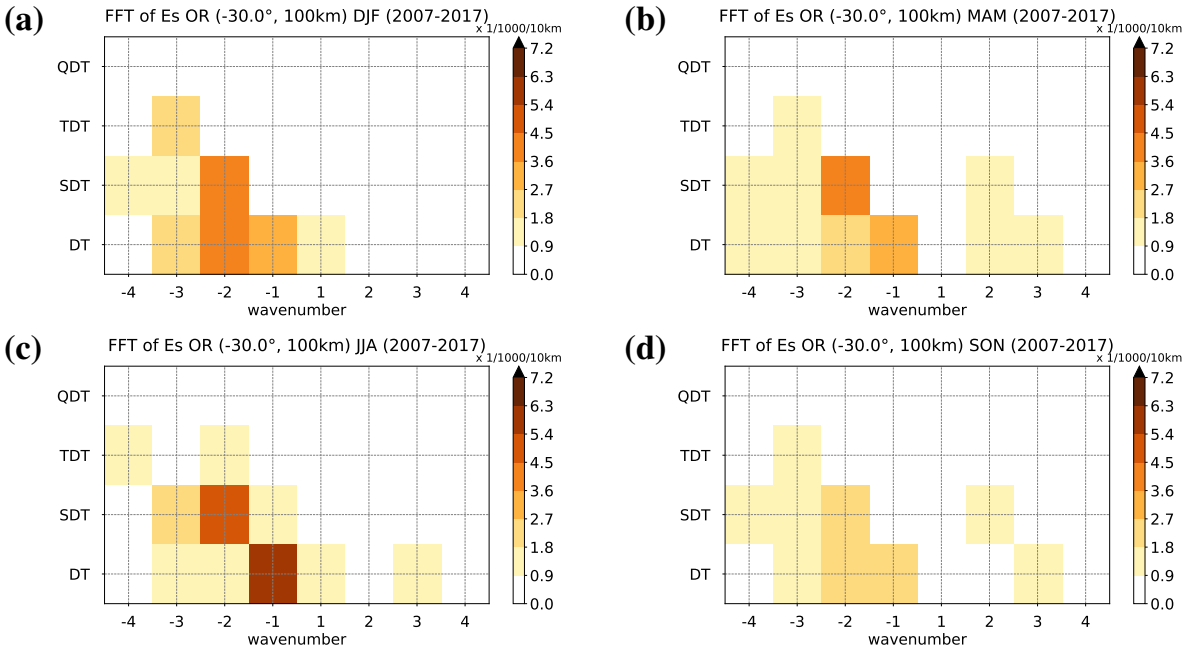

Figure 4: *As in Fig. 3, but at 30°S.*

and only a DW1 is visible. During equinoxes, a TW3 also appears, which reflects the seasonal cycle of the TDT with maximums in autumn/spring and winter (Jacobi et al., 2018a; Lilienthal et al., 2018). The QW4 is weak and only visible in summer. The only relevant non-migrating component is a SW3 signature in summer.

In the SH at 30°S, more non-migrating components show up. In addition to a winter (JJA) SW3, there is a distinct DW2 in all seasons except for winter. The stronger non-migrating components may be owing to the distinct non-zonal structure of overall E_S OR through the South Atlantic Anomaly.

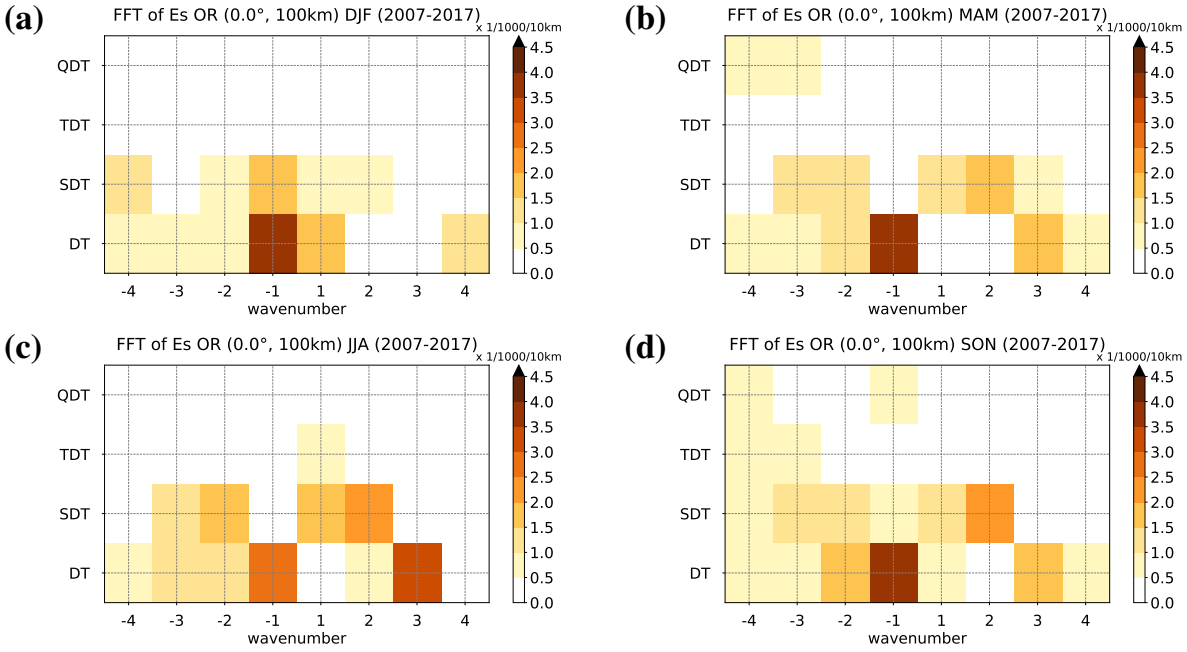

Figure 5: *As in Fig. 3, but at the equator.*

The spectral distribution at the equator shown in Figure 5 differs from the one at midlatitudes. The DW1 is strongest in most months, but during NH summer (JJA) and equinoxes, a clear DE3 is visible, with amplitudes partly larger than the DW1. The DE3 is accompanied by a SE2 during these months. The SE2 is stronger than the rather weak SW2 at the equator. There are several other non-migrating components, namely a DE1 and a SW1 in NH winter (DJF), a SE1 in JJA, and a DW2 in SON. These components may partly be due to the non-zonal structure of the background E_S, especially at the South American Anomaly. TDT and QDT signatures are weak at the equator.

The latitudinal distributions of DT and SDT spectra are shown in Figures 6 and 7. Figure 6 also shows that in the NH the migrating DW1 dominates, in all seasons, while in the SH there is also a DW2 as already visible in Figure 4. At the equator, the DE3 is visible. Note that there is a strong DW1 signature at high latitudes, which is not connected with tidal activity, but due to the action of magnetospheric electric fields (Kirkwood and Nilsson, 2000). The SDT (Figure 7) in the NH is, as is the case with the DT, mainly due to the migrating SW2, except for a summer SW3, which is also seen in the SH summer. In the SH, also the non-migrating SW1 is visible during most of the year.

The latitudinal distributions of TDT and QDT spectra are shown in Figures 8 and 9. Their amplitudes are much weaker than the DT and SDT ones. For the TDT, again the migrating TW3 dominates, but there is a considerable activity of non-migrating components, in particular a TW2, but in some seasons and at some latitudes also a TW4, TW1, and TE1. The QDT is more irregular. The migrating QW4 dominates in most months, but there is also a distinct QW3, QW2, and other components.

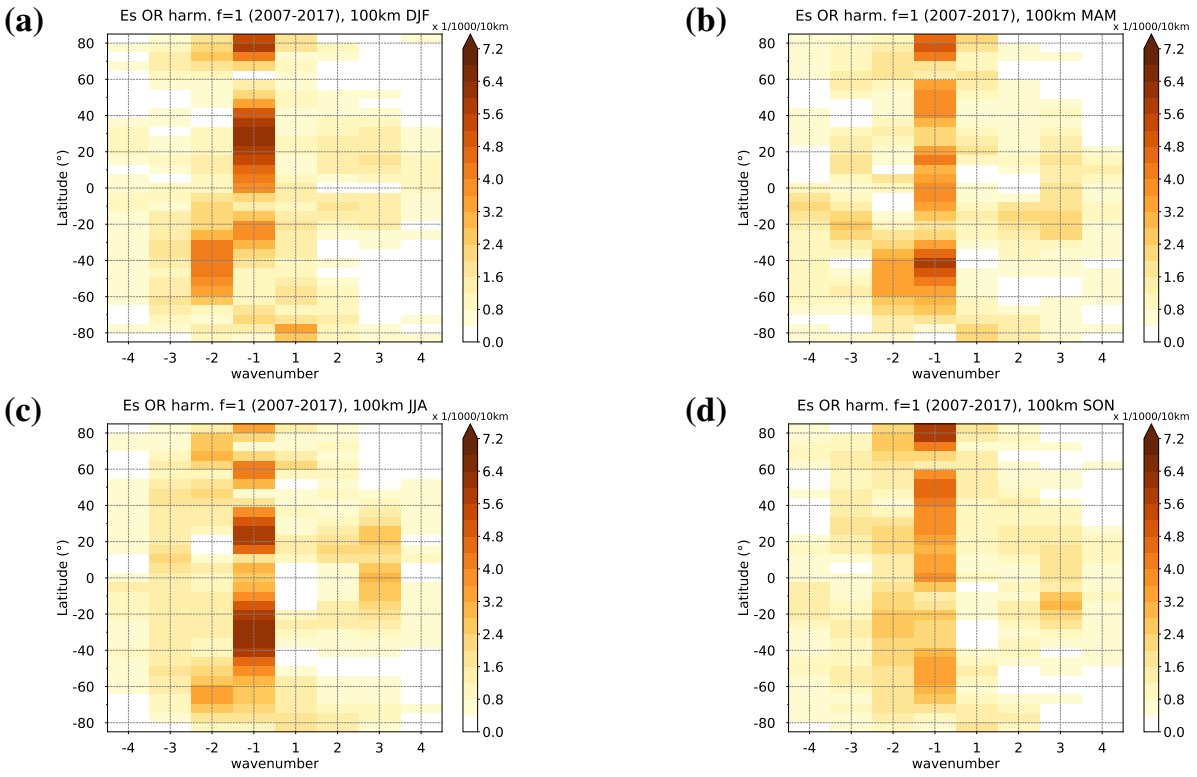

Figure 6: *Global distribution of DT wavenumber spectra of E_S OR in the 95 – 105 km height window for (a) DJF, (b) MAM, (c) JJA, and (d) SON.*

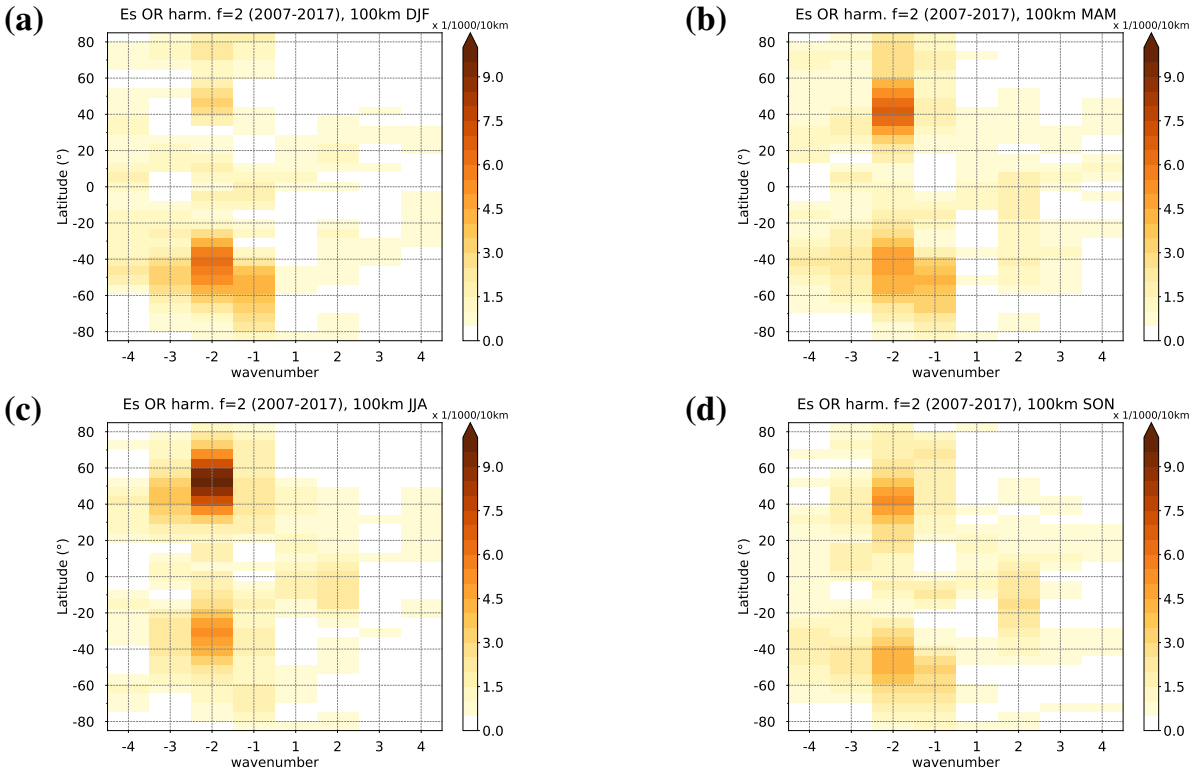

Figure 7: *As in Fig. 6 but for the SDT.*

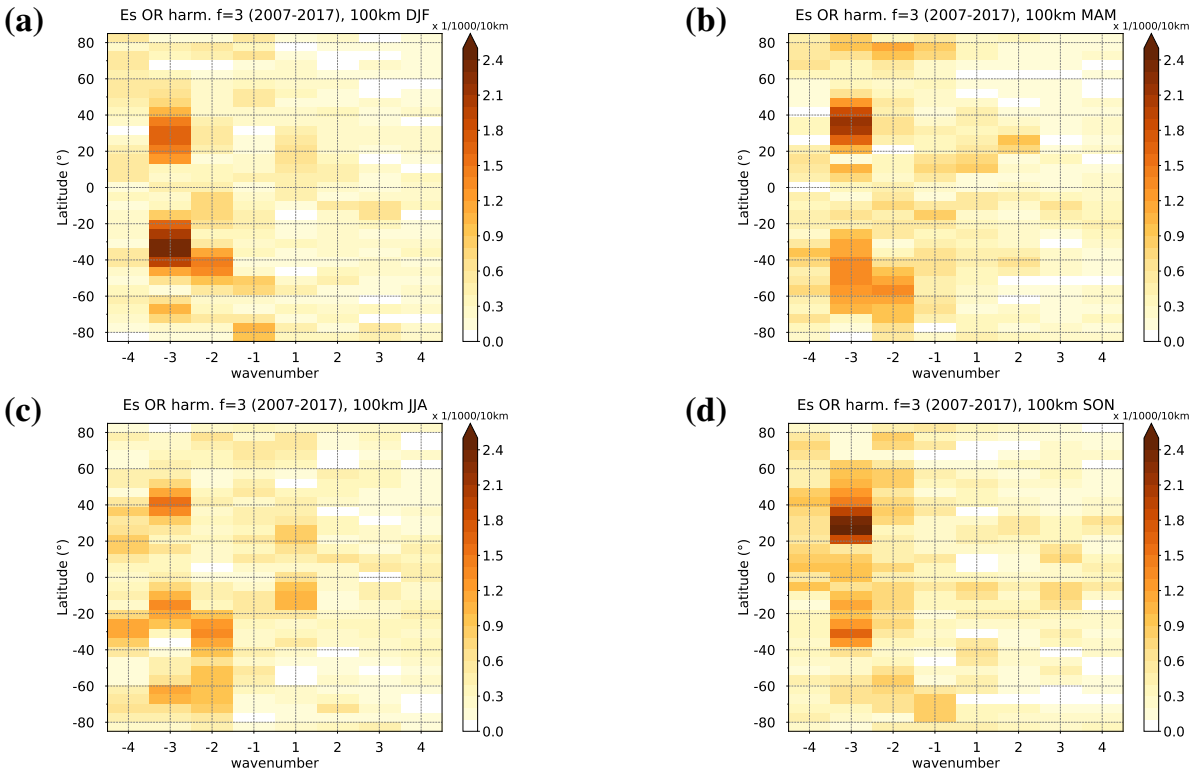

Figure 8: *As in Fig. 6 but for the TDT.*

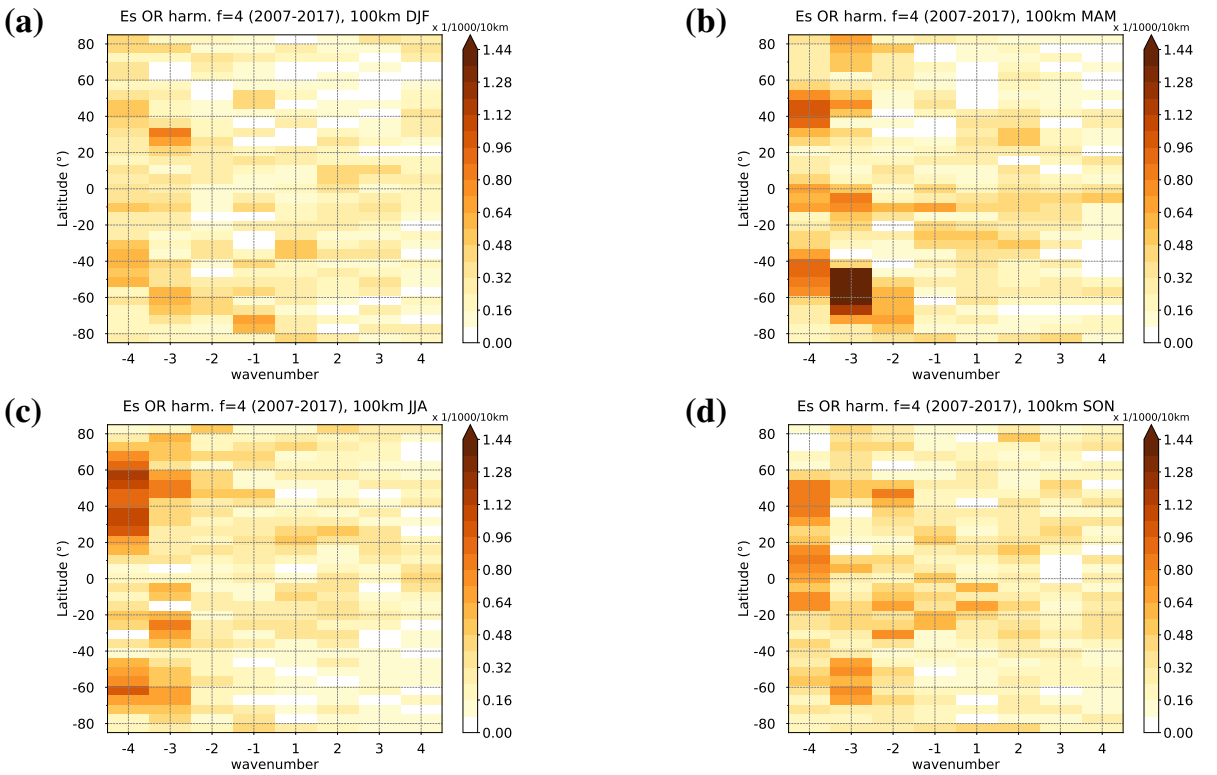

Figure 9: *As in Fig. 6 but for the QDT.*

5 Conclusions & Outlook

We analyzed E_S OR obtained from ionospheric GPS RO. Maximum OR are seen at 95 – 105 km altitude. The strongest signals are due to the migrating DW1 and SW2. Especially in the SH, non-migrating components such as a DW2 and a SW1 are also visible, especially at higher latitudes. Near the equator, a strong DE3 and also a SE2 occur in summer and autumn. Terdiurnal and quarterdiurnal components are weaker than the diurnal and semidiurnal ones.

Note that the amplitudes of OR oscillations, or tidal components in OR, are determined by the tidal activity and the corresponding wind shear, but also by the background ionization of metallic ions. The latter, in particular produces a DW1 signature, but this is not connected with shear, as has been shown by phase comparisons by Jacobi et al. (2018a). Furthermore, the seasonal cycle and global structure of E_S amplitudes also reflect the respective background OR, which are determined by meteor influx (Haldoupis et al., 2007; Jacobi et al., 2013). Removing the background variability by normalizing OR amplitudes by the OR background (e.g., Fytterer et al., 2014; Jacobi et al., 2019) frequently leads to a stronger correspondence of the wind and E_S amplitude distributions.

Acknowledgements: The provision of FORMOSAT-3/COSMIC data by University Corporation for Atmospheric Research is gratefully acknowledged. CJ and FL acknowledge support by Deutsche Forschungsgemeinschaft through grant JA 836/34-1.

References

Anthes, R. A., Bernhardt, P. A., Chen, Y., et al.: The COSMIC/FORMOSAT-3 Mission: Early Results, Bull. Amer. Meteorol. Soc., 89, 313–334, doi:10.1175/BAMS-89-3-313, 2008.

Arras, C. and Wickert, J.: Estimation of ionospheric sporadic E intensities from GPS radio occultation measurements, J. Atmos. Sol.-Terr. Phys., 171, 60 – 63, doi:10.1016/j.jastp.2017.08.006, 2018.

Arras, C., Wickert, J., Beyerle, G., et al.: A global climatology of ionospheric irregularities derived from GPS radio occultation, Geophys. Res. Lett., 35, doi:10.1029/2008GL034158, 2008.

Arras, C., Jacobi, C., and Wickert, J.: Semidiurnal tidal signature in sporadic E occurrence rates derived from GPS radio occultation measurements at higher midlatitudes, Ann. Geophys., 27, 2555–2563, doi:10.5194/angeo-27-2555-2009, 2009.

Arras, C., Jacobi, C., Wickert, J., Heise, S., and Schmidt, T.: Sporadic E signatures revealed from multi-satellite radio occultation measurements, Adv. Radio Sci., 8, 225–230, doi:10.5194/ars-8-225-2010, 2010.

Azeem, I., Walterscheid, R. L., Crowley, G., Bishop, R. L., and Christensen, A. B.: Observations of the migrating semidiurnal and quaddiurnal tides from the RAIDS/NIRS instrument, J. Geophys. Res.: Space Physics, 121, 4626–4637, doi:10.1002/2015JA022240, 2016.

Beldon, C., Muller, H., and Mitchell, N.: The 8-hour tide in the mesosphere and lower thermosphere over the UK, 1988–2004, J. Atmos. Sol.-Terr. Phys., 68, 655–668, doi:10.1016/j.jastp.2005.10.004, 2006.

Chu, Y. H., Wang, C. Y., Wu, K. H., et al.: Morphology of sporadic E layer retrieved from COSMIC GPS radio occultation measurements: Wind shear theory examination, J. Geophys. Res.: Space Physics, 119, 2117–2136, doi:10.1002/2013JA019437, 2014.

Forbes, J. M.: Tidal and Planetary Waves, pp. 67–87, American Geophysical Union (AGU), doi:10.1029/GM087p0067, 1995.

Fytterer, T., Arras, C., and Jacobi, C.: Terdiurnal signatures in sporadic E layers at midlatitudes, Adv. Radio Sci., 11, 333–339, doi:10.5194/ars-11-333-2013, 2013.

Fytterer, T., Arras, C., Hoffmann, P., and Jacobi, C.: Global distribution of the migrating terdiurnal tide seen in sporadic E occurrence frequencies obtained from GPS radio occultations, Earth Planets Space, 66, 1–9, doi:10.1186/1880-5981-66-79, 2014.

Gong, Y., Zhou, Q., and Zhang, S.: Numerical and observational study of ion layer formation at Arecibo, in: XXXIth URSI General Assembly, Beijing, China, pp. 1–4, doi:10.1109/URSIGASS.2014.6929732, 2014.

Guharay, A., Batista, P. P., Buriti, R. A., and Schuch, N. J.: On the variability of the quarter-diurnal tide in the MLT over Brazilian low-latitude stations, Earth Planets Space, 70, 140, doi:10.1186/s40623-018-0910-9, 2018.

Hajj, G., Kursinski, E., Romans, L., Bertiger, W., and Leroy, S.: A technical description of atmospheric sounding by GPS occultation, J. Atmos. Sol.-Terr. Phys., 64, 451 – 469, doi:10.1016/S1364-6826(01)00114-6, 2002.

Haldoupis, C.: Midlatitude Sporadic E. A Typical Paradigm of Atmosphere-Ionosphere Coupling, Space Sci. Rev., 168, 441–461, doi:10.1007/s11214-011-9786-8, 2012.

Haldoupis, C., Meek, C., Christakis, N., Pancheva, D., and Bourdillon, A.: Ionogram height–time–intensity observations of descending sporadic E layers at mid-latitude, J. Atmos. Sol.-Terr. Phys., 68, 539 – 557, doi:10.1016/j.jastp.2005.03.020, 2006.

Haldoupis, C., Pancheva, D., Singer, W., Meek, C., and MacDougall, J.: An explanation for the seasonal dependence of midlatitude sporadic E layers, J. Geophys. Res.: Space Physics, 112, doi:10.1029/2007JA012322, 2007.

Jacobi, C. and Arras, C.: Tidal wind shear observed by meteor radar and comparison with sporadic E occurrence rates based on GPS radio occultation observations, Advances in Radio Science, 17, 213–224, doi:10.5194/ars-17-213-2019, 2019.

Jacobi, C., Portnyagin, Y., Solovjova, T., et al.: Climatology of the semidiurnal tide at 52–56°N from ground-based radar wind measurements 1985–1995, J. Atmos. Sol.-Terr. Phys., 61, 975 – 991, doi:https://doi.org/10.1016/S1364-6826(99)00065-6, 1999.

Jacobi, C., Arras, C., and Wickert, J.: Enhanced sporadic E occurrence rates during the Geminid meteor

showers 2006-2010, Advances in Radio Science, 11, 313–318, doi:10.5194/ars-11-313-2013, 2013.

Jacobi, C., Geißler, C., Lilienthal, F., and Krug, A.: Forcing mechanisms of the 6 h tide in the mesosphere/lower thermosphere, Adv. Radio Sci., 16, 141–147, doi:10.5194/ars-16-141-2018, 2018a.

Jacobi, C., Arras, C., Geißler, C., and Lilienthal, F.: Quarterdiurnal signature in sporadic E occurrence rates and comparison with neutral wind shear, Annales Geophysicae, 37, 273–288, doi:10.5194/angeo-37-273-2019, 2019.

Kirkwood, S. and Nilsson, H.: High-latitude Sporadic-E and other Thin Layers – the Role of Magnetospheric Electric Fields, Space Science Reviews, 91, 579–613, doi:10.1023/A:1005241931650, 2000.

Kursinski, E. R., Hajj, G. A., Schofield, J. T., Linfield, R. P., and Hardy, K. R.: Observing Earth's atmosphere with radio occultation measurements using the Global Positioning System, J. Geophys. Res.: Atmospheres, 102, 23 429–23 465, doi:10.1029/97JD01569, 1997.

Lilienthal, F., Jacobi, C., and Geißler, C.: Forcing mechanisms of the terdiurnal tide, Atmospheric Chemistry and Physics, 18, 15 725–15 742, doi:10.5194/acp-18-15725-2018, 2018.

Liu, H., Tsutsumi, M., and Liu, H.: Vertical Structure of Terdiurnal Tides in the Antarctic MLT Region: 15-Year Observation Over Syowa (69°S, 39°E), Geophysical Research Letters, 46, 2364–2371, doi:https://doi.org/10.1029/2019GL082155, 2019.

Liu, M., Xu, J., Yue, J., and Jiang, G.: Global structure and seasonal variations of the migrating 6-h tide observed by SABER/TIMED, Sci. China Earth Sci., 58, 1216–1227, doi:10.1007/s11430-014-5046-6, 2015.

Mathews, J.: Sporadic E: current views and recent progress, J. Atmos. Sol.-Terr. Phys., 60, 413 – 435, doi:10.1016/S1364-6826(97)00043-6, 1998.

Pancheva, D., Mitchell, N., Hagan, M., et al.: Global-scale tidal structure in the mesosphere and lower thermosphere during the PSMOS campaign of June–August 1999 and comparisons with the global-scale wave model, J. Atmos. Sol.-Terr. Phys., 64, 1011 – 1035, doi:https://doi.org/10.1016/S1364-6826(02)00054-8, 2002.

Resende, L. C. A., Batista, I. S., Denardini, C. M., et al.: The influence of tidal winds in the formation of blanketing sporadic e-layer over equatorial Brazilian region, J. Atmos. Sol.-Terr. Phys., 171, 64 – 71, doi:https://doi.org/10.1016/j.jastp.2017.06.009, 2018a.

Resende, L. C. A., Arras, C., Batista, I. S., et al.: Study of sporadic E layers based on GPS radio occultation measurements and digisonde data over the Brazilian region, Ann. Geophys., 36, 587–593, doi:10.5194/angeo-36-587-2018, 2018b.

Whitehead, J.: The formation of the sporadic-E layer in the temperate zones, J. Atmos. Terr. Phys., 20, 49 – 58, doi:10.1016/0021-9169(61)90097-6, 1961.